CARBON 50 (2012) 637–645

Available at www.sciencedirect.com

SciVerse ScienceDirect

journal homepage: www.elsevier.com/locate/carbon

Edge doping of graphene sheets

Kevin Brenner [a,*], *Yinxiao Yang* [a], *Raghu Murali* [b]

[a] *School of Electrical and Computer Engineering, Georgia Institute of Technology, 777 Atlantic Drive NW, Atlanta, GA 30332, USA*
[b] *Nanotechnology Research Center, Georgia Institute of Technology, 791 Atlantic Drive NW, Atlanta, GA 30332, USA*

ARTICLE INFO

Article history:
Received 26 May 2011
Accepted 8 September 2011
Available online 17 September 2011

ABSTRACT

We present a direct comparison between two fundamental methods of chemically doping the 2-dimensional graphene sheet: (1) passivation of dangling σ-bonds resulting from a vacancy defect and (2) charge transfer from adsorption on the pristine basal plane. Using electron beam lithography and the negative tone resist hydrogen silsesquioxane, we are able to observe the doping contribution from the passivation of such defects that naturally reside along the edge of graphene sheets, and directly compare them to the doping limitations of basal plane adsorption methods. We demonstrate that the passivation of the edge is over three orders of magnitude more efficient for chemical doping than adsorption, in terms of conducting carriers donated per available C-atom. Moreover, as large-area graphene sheets are tailored into nanoscale devices, and the portion of C-atoms that occupy the edge increases, we demonstrate that edge decoration becomes a more pronounced method of chemical doping, exhibiting a scaling law that will induce vast carrier densities and dominance over adsorption techniques in the nanoscale.

1. Introduction

Graphene sheets, a 2-dimensional (2D) allotrope of carbon, have recently drawn enormous attention as a potential candidate for nanoscale electrical conduction applications. High intrinsic mobility [1–3], combined with the ability to modulate the Fermi level [4], allows the conductivity of graphene to be tuned by orders of magnitude. Chemical routes toward doping graphene are highly attractive over electrostatic methods, which require static power dissipation and are limited by dielectric breakdown and stability issues [5,6]. Being a 2D system, graphene requires a departure from 3D bulk semiconductor doping techniques and a rethinking of the most efficient and practical route toward doping the material at nanoscale dimensions. Owing to the graphene sheet being atomically thin, doping techniques that are less intrusive and preserve a pristine lattice are desirable over the direct incorporation of dopant species into the basal plane, which can severely limit mobility [7]. In this work, we show that the passivation of C-atoms residing adjacent to vacancy defects is over three orders of magnitude more efficient a doping mechanism than adsorption on basal plane C-atoms, the metric for comparison being conducting carriers donated per available C-atom. When leveraging naturally occurring edge defects as dopant sites, i.e. broken σ-bonds along edge C-atoms, a scaling law of increased doping with reduced dimensions is observed and will exhibit pronounced control over the carrier density as large-area graphene sheets are scaled into nanometer features.

Most of the doping methods shown to date on graphene operate on the mechanism of surface charge transfer; adsorption or intimate contact on a continuous and nearly vacancy-free basal plane. It has been shown that graphene doping can be induced by interactions with a number of materials such as adsorption of gasses [8], liquids [9], polymers [10], metals [11], and organic molecules [12]. Also, we have demonstrated that thin films of hydrogen silsesquioxane (HSQ) can be used to either n- or p-dope graphene by controlling the amount of

* *Corresponding author:*
E-mail address: kevin.brenner@gatech.edu (K. Brenner).
0008-6223/$ - see front matter
doi:10.1016/j.carbon.2011.09.021

incident energy [13]; the film undergoes a transition from H-rich to O-rich as it cross-links, corresponding to n- and p-doping, respectively.

Intrinsic graphene is thought to have a carrier density of 10^{11} cm^{-2} [4,14]; comparing this to the atomic density of monolayer graphene ($\sim 4 \times 10^{15}$ cm^{-2}), only 1 in 40,000 atoms contribute to conduction at room temperature. Carrier densities on the order of 10^{14} cm^{-2} have been induced by electrostatic doping [15]. Though doping by electrostatic gating is impractical for most applications, it provides evidence that the carrier density in graphene sheets can be increased to more than 1000 times the intrinsic density. Surface charge transfer induces only a weak carrier density in graphene, on the order of 10^{12} cm^{-2}, and is predicted to exhibit an effective charge donated per C-atom on the order of 1×10^{-3}–1×10^{-2} carriers [11,16,17]. Methods of inducing ultrahigh carrier densities in nanoscale graphene sheets, without significant reductions in mobility or requiring static power dissipation are highly sought. The passivation of naturally occurring defects along the edge of cleaved graphene sheets can provide an efficient and potentially effortless chemical doping route for widely tuning the conductance of nanoscale graphene devices. Many predictions have been made on the doping possibilities by graphene edge decoration with various species [18–21]. In addition, the elevated reactivity of the edge has also been studied in relation to the basal plane [22,23], making edge defects a natural candidate for passivation. Along these lines, ammonia doping of fabricated graphene nanoribbons was thought to have a strong edge doping component [24]. Raman studies of diazonium salt functionalization of edges reveal that a defect-related peak (D-peak) at 1350 cm^{-1} is visible at the edges [25], and is attributed to covalent bonding of edge atoms with the doping species. In this work, we provide a direct comparison of the doping efficiency of edge defect sites versus adsorption on basal plane C-atoms on graphene sheets, highlighting intrinsic scaling laws unique to edge defect doping that are predicted to dominate in the nanoscale regime.

2. Experimental

2.1. Graphene sheet preparation

The mechanical exfoliation of the graphene sheets used in this work is carried out under ambient atmospheric conditions, on thermally grown SiO_2 (300 nm) atop a heavily doped Si substrate. Monolayer graphene sheets are first identified by optical contrast then verified using Raman spectroscopy and Atomic Force Microscopy (AFM). A four-point contact metallization pattern is defined using electron beam lithography (EBL), followed by an electron beam (e-beam) evaporation of a Ti/Au metal stack (20 nm/80 nm) and a standard metal lift-off procedure. A short, controlled exposure to a 5 keV e-beam occurs for all graphene sheets during quick scanning electron microscope (SEM) imaging to obtain accurate geometries for subsequent edge patterning. Graphene devices are then pumped for 24 h at a vacuum of 1.5×10^{-6} Torr before four-point electrical testing is performed under vacuum at room temperature to extract the intrinsic material properties. A pulsed-gate bias technique is used to minimize oxide and impurity hysteresis [26], which is verified by performing double sweeps of the gate bias.

A thin film of HSQ atop the graphene sheet is employed to provide both n- and p-doping to either the edge or basal plane [13]. By controlling the degree of cross-linking in the HSQ, n- and p-doped regions can be selectively patterned [27–29]. All graphene sheets go through a spin-on application of HSQ (30 nm), a bake (180 °C) and an application of appropriate dose to the edge and basal plane. The EBL dose is delivered using a JEOL JBX-9300FS 100 keV e-beam operating at a 2 nA beam current with a 4 nm spot diameter; $\sim 1.5 \times 10^4$ A/cm^2 current density. Lastly, the graphene sheets go through a develop in tetramethylammonium hydroxide to remove uncross-linked HSQ. To define an n-doped basal region, a low dose of 200 μC/cm^2 is delivered to the film/graphene stack to avoid e-beam induced damage of graphene while at the same time providing a shift of the Fermi level (~200 meV) into the conduction band. To define a p-doped region, a dose of 2000 μC/cm^2 is used since it sufficiently outgases H from the film, making it O-rich.

All graphene sheets that are compared in this work are subject to identical process conditions to reduce process-induced variability between samples, and have nearly identical widths. After the sheets are tested for their initial (pristine) response and spin-coated with the HSQ thin film, they are processed into two distinct devices: (1) n-doped edge and n-doped basal plane and (2) p-doped edge and n-doped basal plane. These are labeled as NNG and PNG sheets, respectively. For NNG sheets, n-doping is applied to the edge and basal plane by exposing the entire sheet to the uniform low e-beam dose. For PNG, p-doping is selectively applied to the graphene edge by exposing a narrow O-rich HSQ layer along the edge of the sheet to the high e-beam dose while the low dose is still given to the basal plane to induce similar n-doping. A minimal (~200 nm) high dose HSQ overlap onto the basal plane of the PNG sheet is achieved, thereby allowing for an independent study of the edge doping and basal plane doping components. Low-power Raman spectroscopy is performed on both the basal plane and edge of the graphene, Fig. 1. A D-peak in the Raman spectrum is observed exclusively along the edge of the sheet, verifying a finite passivated edge defect population as well as the pristine quality of the basal plane.

2.2. Electrical characterization

Electrical testing on an NNG sheet reveals a significant negative shift in the minimum conductivity point (V_{gmin}) compared to the pristine response, Fig. 2a. This is caused by the charge-transfer from H to the graphene and is consistent with the n-doping previously reported [13,16]. The novelty of this work lies in understanding the behavior of PNG sheets, where the competition between p-doped edges and an n-doped basal plane allows for a direct observation of the role of the edge doping component, Fig. 2b. It can be seen that the PNG sheet displays a reduced shift of V_{gmin} of −8 V. An NNG sheet has an n-doped edge resulting from sp^2 H-passivation of dangling bonds on edge defects, as well as an n-doped basal plane due to adsorption of molecular H_2, Fig. 2c. A PNG sheet has a p-doped edge resulting from O-passivation, and a similar n-doped basal plane resulting from H_2 adsorption, Fig. 2d.

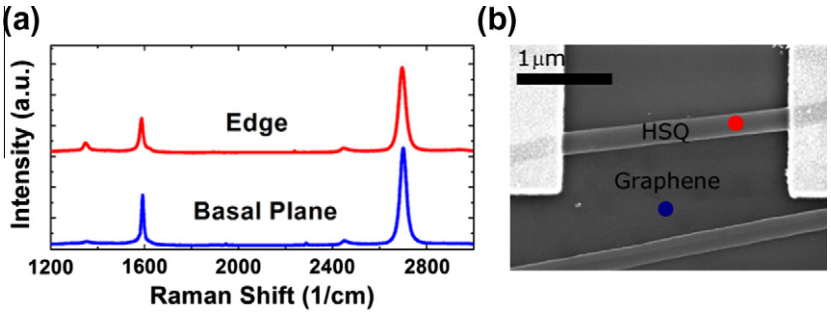

Fig. 1 – (a) Raman spectroscopy is performed on the edge and basal plane of all graphene sheets to identify monolayer graphene. A prominent D-peak is found to emerge exclusively along the edge of the sheet, indicating defects and covalent passivation. (b) An SEM image of a fabricated PNG sheet identifying the edge and basal Raman mapping locations. A thin layer of HSQ selectively cross-linked along the edge of the sheet is visible. A minimal basal plane overlap of ~200 nm is maintained for all PNG sheets.

An SEM image of a PNG sheet with contact metallization is shown in Fig. 2e. A narrow O-rich region of heavily cross-linked HSQ is visible along the sheet edge, inducing O-passivated edge defects. NNG sheets are found to exhibit shifts of V_{gmin} ranging from −40 to −28 V and PNG sheets exhibit shifts from −15 to −3 V. The variation in the pristine doping level of the NNG and PNG sheet is attributed to dopants trapped between the graphene and substrate. Despite thorough cleaning and sufficient dwell time under high vacuum, these doping levels will vary slightly between substrates, yet remain constant throughout processing.

A direct observation of edge doping is obtained by demonstrating NNG and PNG behavior on the same graphene sheet, Fig. 3a. An NNG sheet is compared to its pristine response and found to exhibit a −25 V shift of V_{gmin}. The edge is then transitioned from n- to p-doping via an EBL exposure; similar to all PNG sheets. It is found that by changing the polarity of only the edge doping component, a shift of V_{gmin} of 13 V (~230 meV) is induced. SEM imaging of the NNG and PNG graphene sheet are shown in Fig. 3b and c.

3. Results and discussion

3.1. HSQ doping mechanism

In extracting the doping efficiencies, a detailed understanding of the HSQ doping mechanism is required. The process of spin-coating the HSQ resin precursor ($H_8Si_8O_{12}$) atop the graphene releases approximately 65% of its H-content in the form of volatile molecular H_2 [30]. Since this will diffuse out all surfaces of the film, it is assumed that a flux of H_2 on par with ~30% of the resin's content will reach the graphene surface. For a film thickness of 30 nm, and an HSQ molecular mass of 424 g/mol, the flux of H_2 to the basal plane of the graphene sheet should be on the order of 1×10^{16} cm^{-2}, which is comparable to the atomic density of the graphene lattice. The binding energy of molecular H_2 to the pristine graphene surface should be on the order of 70 meV [31]. Although there is a slight preference (~10 meV) for the molecule to situate in the center of the graphene hexagon, the 200 °C bake of the film to remove solvent provides sufficient energy for overcoming the 14 meV diffusion barrier of H_2 on the graphene sheet, making a uniform adsorption atop basal plane C-atoms likely [31]. Chemical doping via adsorption is the primary mechanism of charge transfer on the basal plane, as indicated by the lack of a significant defect population, verified by spectroscopy in Fig. 1. The 5 keV e-beam exposure that occurs during SEM imaging is over an order of magnitude below the incident energy required for the sputtering of C-atoms [32], and will not generate vacancy defects on the basal plane. Similarly, the 100 kV e-beam of the EBL used to deliver the 200 μC/cm^2 dose to the basal plane is below the ~130 keV threshold for knock-on displacement of sp^2 bonded carbon [33], thus maintaining a pristine, adsorption doped, basal plane. Moreover, the dwell time of the e-beam over basal C-atoms is on the order of 10's of nanoseconds for a 200 μC/cm^2 dose, which is far below the sputtering rate for even 200 keV electrons, which is on par with 1 nm/s [34].

The edge of the graphene sheet is passivated through distinctly different mechanisms for the NNG and PNG sheets, which exhibit n- and p-doped edges, respectively. For the NNG sheet, a partially-decorated H-passivated edge that is n-doped is assumed to result from the exfoliation process [20]. STM measurements of sp^2 hybridized graphite edges in air at room temperature have revealed edges passivated by H [35]. Additionally, the spontaneous disassociation of gaseous molecular H_2 and water vapor to form H-passivated edge defects has been shown to occur exothermically through a number of possible scenarios [36,37]. Graphene sheet edges cleaved under ambient conditions with typical partial pressures of molecular H_2 preferably form sp^2 bonding [38]. The sp^2 H-passivated NNG edge that exists will donate unpaired electrons for conduction [18,39]. The PNG O-passivated, p-doped, edge is generated through the process of replacing H with O at passivated edge C-atom sites. This transition occurs through the mechanism of knock-on displacement of light H-atoms passivating the ribbon edge, which takes place at electron energies below the threshold for C-atom displacement [40]; i.e. H can be displaced while maintaining the graphene lattice. A similar mechanism of irradiation-induced selective expulsion of H from C-films was previously demonstrated using ion irradiation [41]. The 2000 μC/cm^2 dose that is applied to the edge of the PNG sheet effectively outgases H from

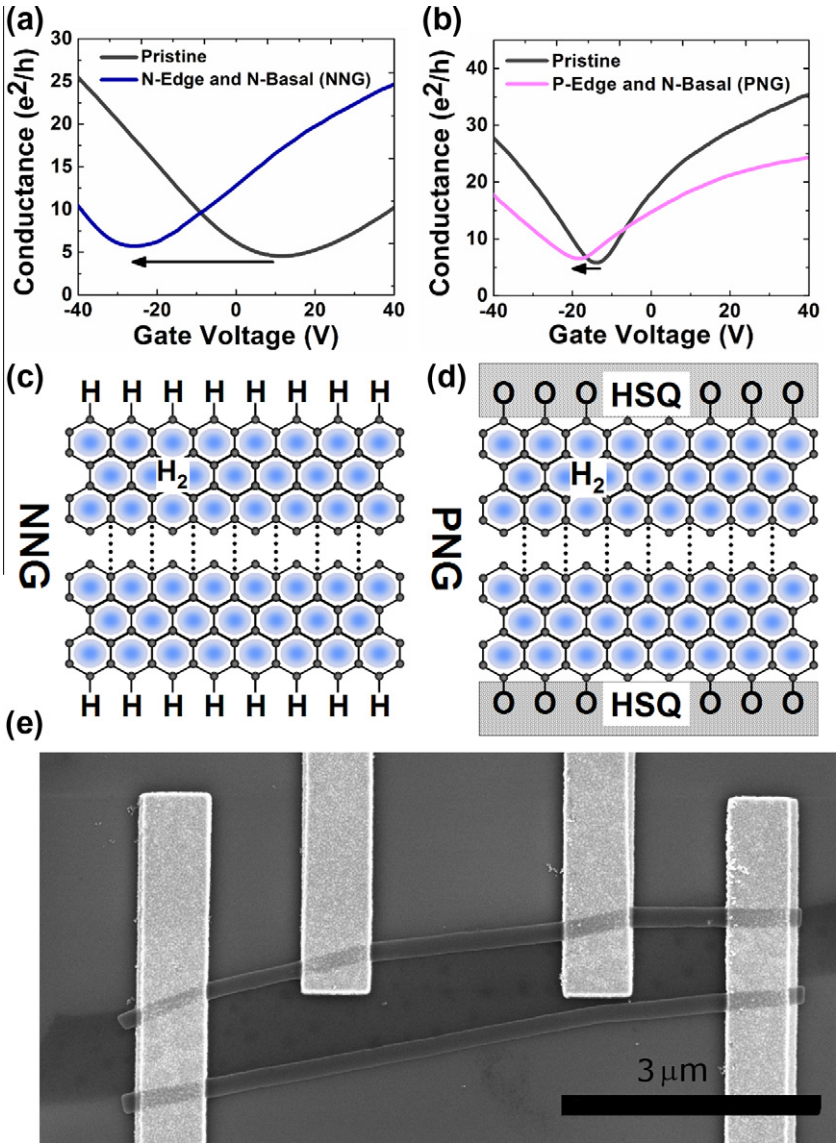

Fig. 2 – (a) Four-point electrical testing under vacuum of a graphene sheet with an n-doped edge and basal plane (NNG). A shift of V_{gmin} of −35 V from its pristine doping is observed. (b) Electrical testing of a graphene sheet with a p-doped edge and n-doped basal plane (PNG) exhibits a reduced shift of V_{gmin} of −8 V. This reduction is attributed to the competing p-doping contribution from the edge passivation. (c) An NNG sheet is described as having a uniform basal plane adsorption of molecular H_2, inducing an n-doped basal plane. Hydrogen passivation along the edge of the NNG induces an n-doped edge. (d) A PNG sheet is described as similarly having an n-doped basal plane resulting from molecular H_2 adsorption, however a thin film of heavily cross-linked HSQ along the edge passivates dangling bonds with O, inducing a p-doped edge. (e) An SEM image of a PNG sheet with contact metallization.

the HSQ film, which facilitates the transition from a H- to O-rich environment around the freshly de-passivated edge C-atoms [28]. The passivation of dangling σ-bonds along the edge of the graphene sheet with O has been studied previously and should contribute p-carriers to the conducting graphene π-system [42].

Regarding the extent of doping at the graphene edge, only a fraction of total available edge C-atoms will contribute to chemical doping; i.e. a mixed edge exists [43]. The instant the graphene edge is cleaved during the exfoliation process, which is identical for all NNG and PNG sheets, it is assumed that a fixed, and finite, population of edge C-atoms passivate with foreign species from the ambient environment or remain chemically reactive, whereas the remainder will become chemically inert through the process of C–C edge reconstruction. There are two primary mechanisms that govern the extent of edge passivation. The first is the fraction of the graphene edge that orients with a zigzag chirality, since this is the only edge state that is predicted to facilitate chemical passivation due to the large density of states near the Fermi level, which is absent for other orientations [44–46]. The second is the availability of potential passivating species, whose absence would result in an entirely reconstructed edge, as observed by STM imaging under vacuum [47]. Based

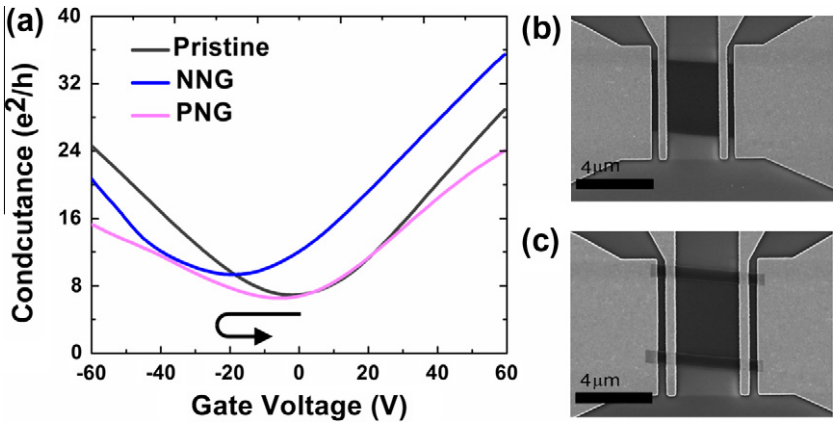

Fig. 3 – (a) A direct observation of the doping from edge C-atoms is extracted from the same graphene sheet. A pristine graphene sheet is doped with an n-typed edge and basal plane (NNG) and found to exhibit a shift of V_{gmin} by −25 V. The edge is then transitioned from n- to p-doping (PNG) by exposing an O-rich HSQ region selectively along the edge of the same graphene sheet. By switching the doping polarity of the edge, a V_{gmin} of −12 V is observed. The reduced n-doping is again attributed to the competing p-doping from the edge passivation. (b) SEM imaging of the graphene NNG sheet. (c) SEM imaging of the same graphene sheet as PNG. A thin layer of HSQ is observed along the edge.

on an abundance of ultrahigh resolution STM and tunneling electron microscopy (TEM) imaging of graphene and sp^2 hybridized graphitic edges cleaved in an identical manner to those produced in this work, approximately 30% of the graphene edge will oriented as zigzag [35,39,48–52]. Graphene edges with a zigzag orientation have been shown to be highly chemically reactive and energetically unstable when un-passivated, making them subject to spontaneous and relatively effortless passivation with dopant species [22,25]. Therefore, all edge C-atoms residing on zigzag portions of the sheet edge are expected to contribute to chemical doping.

The fraction of edge C-atoms participating in chemical doping is defined by the exfoliation process, which is identical for NNG and PNG sheets, and expected to remain fixed throughout the subsequent fabrication steps. The electron energies used to irradiate the graphene edge are below the values required for sputtering of C-atoms along the graphene edge or milling a new edge orientation into the sheet [32,33]. We have verified this by exposing the HSQ-coated basal plane of a graphene sheet to the same e-beam dose used at the edge, and observed the maintenance of a pristine, defect barren, basal plane via Raman spectroscopy. The production of the PNG sheet involves the replacing of previously H-passivated edge sites with O, producing a p-type edge; thus the extent of edge doping is similar for both NNG and PNG sheets. With both sp^2 H and O passivation predicted to contribute 1 carrier per passivated C-atom [18,42], similar doping levels should exist for the NNG and PNG sheet edge.

3.2. *The dimensional scaling of edge doping*

The intrinsic n-type edge of the graphene sheet is experimentally observed on pristine devices, where a scaling law of increased doping with a reduction in dimension should exist. Multiple pristine graphene sheets of varying dimension are fabricated on two separate substrates (defined as a batch). The position of the Fermi level (E_f) is carefully extracted and plotted as a function of the sheet's width, Fig. 4. All substrates are thoroughly cleaned before the application of the exfoliated graphene sheets. Once applied, the sheets are cleaned using a copious solvent rinse, and then placed under a vac-

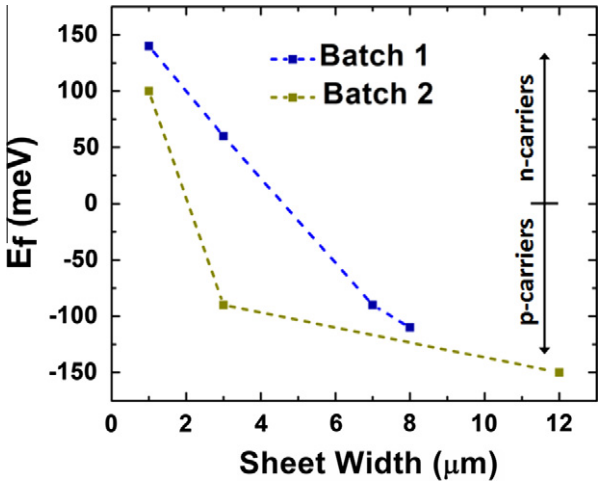

Fig. 4 – Four-point electrical testing under vacuum of pristine graphene sheets fabricated on two separate substrates. The Fermi level positions (doping) for sheets on the same substrate, defined as a batch, are plotted as a function of the graphene sheet width. It is found that a trend of increased n-doping with reduction of width is observable. The n-doping is attributed to H passivation of dangling σ-bonds which occurs during the exfoliation of the graphene ribbons in the ambient environment. Since the number of edge atoms stays relatively fixed regardless of the width, the induced n-carrier density from the edge passivation increases with reduced dimensions. A cross-over from the graphene sheet being dominated by the background p-type doping on the basal plane to the n-type doping from the edge is observed as the width is reduced. This trend should exhibit an order of magnitude increase in the edge doping component with every 10 times reduction in sheet width.

uum of 1.5×10^{-6} T for 24 h before performing 4-point electrical testing at room temperature. Due to limitations in the exfoliation process, obtaining more than four high-quality graphene samples within a batch is difficult to achieve. A scaling law characteristic of edge doping, p- to increasingly stronger n-doping as the n-type edge gains dominance, is observed for all graphene sheets within a batch. The apparent background p-doping on the basal plane is attributed to adsorbates from the ambient environment [4], possibly pinned between the substrate and graphene sheet, whose doping contribution changes between batches, but is found to remain relatively constant within a batch; exhibiting similar values for flakes of similar dimensions but at different locations on the substrate.

3.3. *Charge donation efficiencies*

A model is developed to extract the charge donation efficiency for edge and basal C-atoms, based on the observed shift of V_{gmin} from multiple fabricated NNG and PNG sheets, Fig. 2. All sheets were chosen to have a nearly identical width of 2.2 μm, defined by the exfoliation process. The length of the graphene sheet is defined by the contact metallization spacing, which is set at 3 μm to avoid doping from the adhesion layer metal into a signification portion of the graphene channel [53,54]. Initially an entirely zigzag chirality is assumed for the orientation of the sheet edge. The total number of edge and basal plane C-atoms for the graphene sheet are extracted based on the chaining of an edge and basal unit cell, which dictates eight C-atoms per 0.983 nm of edge length and 16 C-atoms per 0.4217 nm^2 of basal plane, respectively. These values are derived using a 2.46 A lattice constant for the hexagonal C-sheet [55].

The extent of doping along the graphene edge is added to the complexity of the model by scaling back the number of edge atoms that are predicted to contributed to chemical doping; i.e. passivate. First, the effect of edge roughness is accounted for by scaling up the number of available edge C-atoms by a factor of 1.5 to account for added surface area along the contours of the cleaved edge. Second, the number of contributing edge C-atoms is scaled down by a factor of 0.3 to account only for portions of the graphene edge that orient with a zigzag chirality, which is the only orientation expected to facilitate passivation [44–46]. Both of these values are extracted based on a large sampling of high resolution STM and TEM imaging of graphene and graphitic edges produced in a similar manner to all graphene sheets used in this work [35,39,48–52].

The purpose of developing this model is to extract the doping efficiency for edge (χ_E) and basal (χ_B) C-atoms, in a metric of carriers donated per C-atom, based on experimentally observed shifts in the bulk carrier density between NNG and PNG sheets. By observing the role the edge plays in suppressing the n-type doping for a PNG, resulting from the competing polarity of the p-type edge and n-type basal plane, such an extraction can be made. The total carrier density in the graphene sheet (n_{sheet}) can be expressed as the joint contribution of the basal and edge component:

$$n_{sheet} = n_{edge} \pm n_{basal} \quad (1)$$

where,

$$n_{edge} = atoms_E \cdot \chi_E \quad (2)$$

$$n_{basal} = atoms_B \cdot \chi_B \quad (3)$$

Here, $atoms_E$ and $atoms_B$ represent the total contributing edge and basal plane C-atoms, respectively. For NNG sheets, the edge and basal component sum, while for PNG sheets these components subtract. The carrier density is tied to the position of V_{gmin} through the relation: $C_{ox} \cdot V_{gmin} = e \cdot n$, where C_{ox} in the devices produced in this work is 11.6 nF cm^{-2} for 300 nm of SiO_2. For PNG devices, an approximate 200 nm overlap of the cross-linked HSQ onto the basal plane of the sheet, verified by ultrahigh resolution SEM, is taken into account by reducing the n-type basal region, and adding a finite p-doped basal region [13]. A range of likely basal plane efficiencies, based on previously reported predictions for adsorption, from 1×10^{-5} to 1×10^{-3} carriers per C-atom is initially assigned to χ_B [11,16,17]. For each specific estimate for χ_B, the corresponding value of χ_E that produces the observed bulk carrier density in the graphene sheet can be determined. The result is a solution set of unique pairs of χ_E and χ_B, spanning all values of χ_B that fall within the predicted basal plane adsorption range. These solution sets are produced for both NNG and PNG sheets. For NNG sheets, a range of V_{gmin} shifts from −40 V to −28 V was observed, with the mean falling at −34 V. For PNG sheets, a range from −15 V to −3 V is used, with the mean falling at −9 V. The true values of χ_E and χ_B lie at the intersection of the NNG and PNG curves, i.e. the χ pairs that satisfy the observed behavior of both type sheets, Fig. 5.

The spread of projected values for χ_e and χ_b is indicated by the intersection of the solutions for the PNG and NNG sheets, indicated in bold outline in Fig. 5. The true χ values are taken at the intersection for the mean curves for both sheets, indicated with a dot. The results in Fig. 5 reveal that the passivation of C-atoms residing adjacent to vacancy defects contribute close to .85 carriers per C-atom, while adsorption atop basal plane C-atoms contributes close to 5.5×10^{-4} carriers per C-atom. This makes the passivation of edge defects over three orders of magnitude more efficient than basal plane adsorption, as a route towards chemical doping. The value obtained for χ_e lies close to the expected value, which should reside around one carrier per atom for sp^2 H- and O-passivation [18,42]. A strict upper limit on the potential for edge passivation is indicated in red, with two carriers per atom being possible through the pyrollic N-passivation of graphene defects [56]. Donation efficiencies beyond this value are unlikely. Similarly, edge charge donations below 0 carriers per atom represent χ pairs that are not possible for PNG sheets. The extremes of the model do slightly predict values residing in these forbidden ranges, this error is related to variability in the experimental fabrication arising from minor deviations in width of the graphene sheets and basal plane overlap of the cross-linked HSQ on PNG sheets. An estimation of χ is also extracted from the wider graphene sheet in Fig. 3 and found to lie within the outlined spread in Fig. 5; with χ_E predicted to be 1.1 carriers per C-atom. This wider sheet behaves as expected, with the edge having less influence on the overall carrier density; a lower n-doping for the NNG sheet and a weaker shift from the p-doped edge of the PNG.

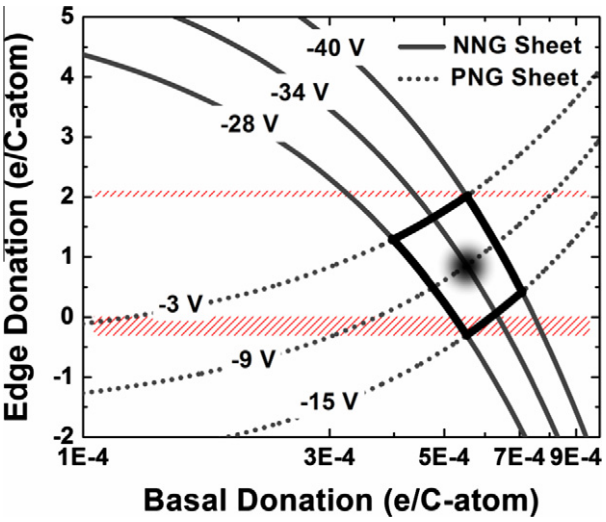

Fig. 5 – The extraction of the charge donated per C-atom for the edge and basal plane (χ_E and χ_B). Based on the experimentally observed shift of V_{gmin} for multiple NNG and PNG sheets, curves representing all pairs of χ_E and χ_B that could produce the observed doping level in the sheet are plotted. NNG sheets are plotted for the experimentally observed span of shifts from −40 to −28 V, with the mean falling at −34 V. PNG sheets are plotted for shifts ranging from −15 to −3 V, with the mean falling at −9 V. The intersection of the NNG and PNG curves, outlined in bold, represents the possible values for χ. The true values for χ_E and χ_B are taken as the intersection of the mean curves, marked with a dot. It is found that charge donation for adsorption atop a basal atom is on the order of 5.5×10^{-4} carriers per C-atom and 0.85 carriers per C-atom for edge atoms. This indicates that edge atoms, or C-atoms residing adjacent to vacancy defects, are over three orders of magnitude more efficient than basal plane atoms as a route towards chemical doping.

The values of χ_E and χ_B can be similarly extracted from the scaling law identified on pristine graphene sheets of varying widths, Fig. 4. Based on the observed shift of E_f as the graphene sheet dimensions are reduced, and assuming that similar basal plane doping exists for all devices within a batch, the contribution of edge and basal atoms is calculated using an iterative method. It is found that for both batches, the value of χ_E converges to a range of 0.5–1 carrier per edge C-atom, while χ_B converges to a range of 0.5–2×10^{-4} carriers per basal C-atom. These χ values are slightly less than those estimated from the NNG and PNG sheets. The difference is a result of changing the basal plane dopant species between the pristine graphene and HSQ-doped (NNG/PNG) sheets. The basal plane of the pristine graphene sheets is expected to be doped by O and atmospheric adsorbents [4]. The efficiency of basal plane doping is dependent on how close the dopant molecule is to the surface of graphene [31]. The adsorption of H for the NNG and PNG sheets is expected to have a more intimate contact with the basal plane of the graphene sheet than atmospheric adsorbates [17], Fig. 4, resulting in more efficient doping. An underestimation of the basal plane doping efficiency for pristine sheets results in a similar under estimation of the edge doping component. Despite these variations in the estimates for χ_E and χ_B, the passivation of edge defects is still predicted to be over three orders of magnitude more efficient. This scaling law, observed in Fig. 4, is unique to edge doping and is highly desirable as a combatant to the onset of LER-limited mobility at narrow dimensions [57]. Based on the analysis presented in this work, a single passivated edge C-atom could provide the equivalent carrier injection to that of adsorption atop a 7 nm× 7 nm basal plane region. Additionally, this work highlights the necessity of carefully controlling the edge chemistry in nanoscale graphene devices. The heightened reactivity of the graphene edge in comparison to the basal plane makes it an attractive candidate for effortless chemical doping [22,25], both deliberately and unintentionally. As large area sheets are patterned into nanometer features, variability in the edge passivation can begin to significantly impact the bulk carrier density, resulting in conductance modifications. Plasma etching techniques can provide interesting avenues for controlling and exploiting the edge chemistry of etched graphene devices.

4. Conclusions

We have directly probed two fundamental routes for chemically doping graphene sheets and shown that passivation of dangling σ-bonds from vacancy defect sites is inherently over 1000-fold more efficient than adsorption on a defect-free graphene lattice, in terms of carriers donated per contributing C-atom. We have carefully extracted the chemical doping efficiencies of edge and basal atoms, in a metric of carriers donated per C-atom and present values of 0.85 and 5.5×10^{-4}, respectively. Using electron beam lithography for edge passivation, the interplay between doping via edge C-atoms and the basal plane adsorption was directly observed on the same graphene sheet. The leveraging of naturally occurring defect sites along the edge of a cleaved or etched graphene sheet exhibits an inherent scaling law of increased doping with reduced dimensions; carrier density growing by an order of magnitude with every 10 times reduction in width. This trend, observed here experimentally on pristine graphene, will induce large carrier densities at nanoscale widths, making it dominant over other chemical doping methods. This work demonstrates the capability of naturally occurring defect sites along the edge of graphene sheets to provide a route towards ultra-high carrier densities in nanoscale graphene systems requiring high conductance.

Acknowledgments

The authors would like to thank Dr. James Meindl for his visionary role in this work. This work is supported by the Semiconductor Research Corporation and Defense Advance Research Projects Agency (DARPA) through the Interconnect Focus Center, and the National Science Foundation (ECCS Grant No. 1001986).

REFERENCES

[1] Bolotin KI, Sikes KJ, Jiang Z, Klima M, Fudenberg G, Hone J, et al. Ultrahigh electron mobility in suspended graphene. Solid State Commun 2008;146(9–10):351–5.
[2] Morozov SV, Novoselov KS, Katsnelson MI, Schedin F, Elias DC, Jaszczak JA, et al. Giant intrinsic carrier mobilities in graphene and its bilayer. Phys Rev Lett 2008;100(1).
[3] Hwang EH, Adam S, Das Sarma S. Carrier transport in two-dimensional graphene layers. Phys Rev Lett 2007;98(18).
[4] Novoselov KS, Geim AK, Morozov SV, Jiang D, Zhang Y, Dubonos SV, et al. Electric field effect in atomically thin carbon films. Science 2004;306(5696):666–9.
[5] Das A, Pisana S, Chakraborty B, Piscanec S, Saha SK, Waghmare UV, et al. Monitoring dopants by Raman scattering in an electrochemically top-gated graphene transistor. Nat Nanotechnol 2008;3(4):210–5.
[6] Efetov DK, Kim P. Controlling electron–phonon interactions in graphene at ultrahigh carrier densities. Phys Rev Lett 2010;105(25).
[7] Wei DC, Liu YQ, Wang Y, Zhang HL, Huang LP, Yu G. Synthesis of n-doped graphene by chemical vapor deposition and its electrical properties. Nano Lett 2009;9(5):1752–8.
[8] Schedin F, Geim AK, Morozov SV, Hill EW, Blake P, Katsnelson MI, et al. Detection of individual gas molecules adsorbed on graphene. Nat Mater 2007;6(9):652–5.
[9] Chen F, Xia JL, Tao NJ. Ionic screening of charged-impurity scattering in graphene. Nano Lett 2009;9(4):1621–5.
[10] Farmer DB, Golizadeh-Mojarad R, Perebeinos V, Lin YM, Tulevski GS, Tsang JC, et al. Chemical doping and electron-hole conduction asymmetry in graphene devices. Nano Lett 2009;9(1):388–92.
[11] Pi K, McCreary KM, Bao W, Han W, Chiang YF, Li Y, et al. Electronic doping and scattering by transition metals on graphene. Phys Rev B 2009;80(7).
[12] Coletti C, Riedl C, Lee DS, Krauss B, Patthey L, von Klitzing K, et al. Charge neutrality and band-gap tuning of epitaxial graphene on SiC by molecular doping. Phys Rev B 2010;81(23).
[13] Brenner K, Murali R. Single step, complementary doping of graphene. Appl Phys Lett 2010;96(6).
[14] Fang T, Konar A, Xing HL, Jena D. Carrier statistics and quantum capacitance of graphene sheets and ribbons. Appl Phys Lett 2007;91(9).
[15] Pachoud A, Jaiswal M, Kailian A, Priscilla; L P K, Oezyilmaz B. Graphene transport at high carrier densities using a polymer electrolyte gate. arxiv:10093367 2010
[16] Ryu S, Han MY, Maultzsch J, Heinz TF, Kim P, Steigerwald ML, et al. Reversible basal plane hydrogenation of graphene. Nano Lett 2008;8(12):4597–602.
[17] Leenaerts O, Partoens B, Peeters FM. Adsorption of H_2O, NH_3, CO, NO_2, and NO on graphene: a first-principles study. Phys Rev B 2008;77(12).
[18] Boukhvalov DW, Katsnelson MI. Chemical functionalization of graphene with defects. Nano Lett 2008;8(12):4373–9.
[19] Biel B, Triozon F, Blase X, Roche S. Chemically induced mobility gaps in graphene nanoribbons: a route for upscaling device performances. Nano Lett 2009;9(7):2725–9.
[20] Cervantes-Sodi F, Csanyi G, Piscanec S, Ferrari AC. Edge-functionalized and substitutionally doped graphene nanoribbons: electronic and spin properties. Phys Rev B 2008;77(16).
[21] Wang ZF, Li QX, Zheng HX, Ren H, Su HB, Shi QW, et al. Tuning the electronic structure of graphene nanoribbons through chemical edge modification: a theoretical study. Phys Rev B 2007;75(11).
[22] Sharma R, Baik JH, Perera CJ, Strano MS. Anomalously large reactivity of single raphene layers and edges toward electron transfer chemistries. Nano Lett 2010;10(2):398–405.
[23] Jiang DE, Sumpter BG, Dai S. Unique chemical reactivity of a graphene nanoribbon's zigzag edge. J Chem Phys 2007;126(13).
[24] Wang XR, Li XL, Zhang L, Yoon Y, Weber PK, Wang HL, et al. n-Doping of graphene through electrothermal reactions with ammonia. Science 2009;324(5928):768–71.
[25] Lim H, Lee JS, Shin HJ, Shin HS, Choi HC. Spatially resolved spontaneous reactivity of diazonium salt on edge and basal plane of graphene without surfactant and its doping effect. Langmuir 2010;26(14):12278–84.
[26] Estrada D, Dutta S, Liao A, Pop E. Reduction of hysteresis for carbon nanotube mobility measurements using pulsed characterization. Nanotechnology 2010;21(8).
[27] Albrecht MG, Blanchette C. Materials issues with thin film hydrogen silsesquioxane low K dielectrics. J Electrochem Soc 1998;145(11):4019–25.
[28] Yang CC, Chen WC. The structures and properties of hydrogen silsesquioxane (HSQ) films produced by thermal curing. J Mater Chem 2002;12(4):1138–41.
[29] Lee HJ, Lin EK, Wang H, Wu WL, Chen W, Moyer ES. Structural comparison of hydrogen silsesquioxane based porous low-k thin films prepared with varying process conditions. Chem Mater 2002;14(4):1845–52.
[30] Loboda MJ, Grove CM, Schneider RF. Properties of a-SiOx: H thin films deposited from hydrogen silsesquioxane resins. J Electrochem Soc 1998;145(8):2861–6.
[31] Arellano JS, Molina LM, Rubio A, Alonso JA. Density functional study of adsorption of molecular hydrogen on graphene layers. J Chem Phys 2000;112(18):8114–9.
[32] Egerton RF, Li P, Malac M. Radiation damage in the TEM and SEM. Micron 2004;35(6):399–409.
[33] Ajayan PM, Ravikumar V, Charlier JC. Surface reconstructions and dimensional changes in single-walled carbon nanotubes. Phys Rev Lett 1998;81(7):1437–40.
[34] Egerton RF, Wang F, Crozier PA. Beam-induced damage to thin specimens in an intense electron probe. Microsc Microanal 2006;12(1):65–71.
[35] Niimi Y, Matsui T, Kambara H, Tagami K, Tsukada M, Fukuyama H. Scanning tunneling microscopy and spectroscopy of the electronic local density of states of graphite surfaces near monoatomic step edges. Phys Rev B 2006;73(8).
[36] Sha XW, Jackson B. The location of adsorbed hydrogen in graphite nanostructures. J Am Chem Soc 2004;126(40):13095–9.
[37] Wassmann T, Seitsonen AP, Saitta AM, Lazzeri M, Mauri F. Structure, stability, edge states, and aromaticity of graphene ribbons. Phys Rev Lett 2008;101(9).
[38] Lu YH, Wu RQ, Shen L, Yang M, Sha ZD, Cai YQ, et al. Effects of edge passivation by hydrogen on electronic structure of armchair graphene nanoribbon and band gap engineering. Appl Phys Lett 2009;94(12).
[39] Kobayashi Y, Fukui K, Enoki T, Kusakabe K. Edge state on hydrogen-terminated graphite edges investigated by scanning tunneling microscopy. Phys Rev B 2006;73(12).
[40] Banhart F. Irradiation effects in carbon nanostructures. Rep Prog Phys 1999;62(8):1181–221.
[41] Barshilia HC, Sah S, Mehta BR, Vankar VD, Avasthi DK, Jaipal, et al. Microstructural modifications in diamond-like carbon thin-films caused by high-energy ion irradiation. Thin Solid Films 1995;258(1–2):123–7.
[42] Zheng HX, Duley W. First-principles study of edge chemical modifications in graphene nanodots. Phys Rev B 2008;78(4).
[43] Nakada K, Fujita M, Dresselhaus G, Dresselhaus MS. Edge state in graphene ribbons: nanometer size effect and edge shape dependence. Phys Rev B 1996;54(24):17954–61.
[44] Stein SE, Brown RL. Pi-electron properties of large condensed polyaromatic hydrocarbons. J Am Chem Soc 1987;109(12):3721–9.

[45] Tanaka K, Yamashita S, Yamabe H, Yamabe T. Electronic-properties of one-dimensional graphite family. Synthetic Met 1987;17(1–3):143–8.
[46] Fujita M, Wakabayashi K, Nakada K, Kusakabe K. Peculiar localized state at zigzag graphite edge. J Phys Soc Jpn 1996;65(7):1920–3.
[47] Girit CO, Meyer JC, Erni R, Rossell MD, Kisielowski C, Yang L, et al. Graphene at the edge: stability and dynamics. Science 2009;323(5922):1705–8.
[48] Kobayashi Y, Fukui K, Enoki T, Kusakabe K, Kaburagi Y. Observation of zigzag and armchair edges of graphite using scanning tunneling microscopy and spectroscopy. Phys Rev B 2005;71(19).
[49] Ritter KA, Lyding JW. The influence of edge structure on the electronic properties of graphene quantum dots and nanoribbons. Nat Mater 2009;8(3):235–42.
[50] Giunta PL, Kelty SP. Direct observation of graphite layer edge states by scanning tunneling microscopy. J Chem Phys 2001;114(4):1807–12.
[51] Niimi Y, Matsui T, Kambara H, Tagami K, Tsukada M, Fukuyama H. Scanning tunneling microscopy and spectroscopy studies of graphite edges. Appl Surf Sci 2005;241(1–2):43–8.
[52] Gupta AK, Russin TJ, Gutierrez HR, Eklund PC. Probing graphene edges via Raman scattering. Acs Nano 2009;3(1):45–52.
[53] Giovannetti G, Khomyakov PA, Brocks G, Karpan VM, van den Brink J, Kelly PJ. Doping graphene with metal contacts. Phys Rev Lett 2008;101(2).
[54] Mueller T, Xia F, Freitag M, Tsang J, Avouris P. Role of contacts in graphene transistors: a scanning photocurrent study. Phys Rev B 2009;79(24).
[55] Wallace PR. The band theory of graphite. Phys Rev 1947;71(9):622–34.
[56] Shao YY, Zhang S, Engelhard MH, Li GS, Shao GC, Wang Y, et al. Nitrogen-doped graphene and its electrochemical applications. J Mater Chem 2010;20(35):7491–6.
[57] Fang T, Konar A, Xing H, Jena D. Mobility in semiconducting graphene nanoribbons: phonon, impurity, and edge roughness scattering. Phys Rev B 2008;78(20).